CHAPTER 5
NEOTECTONICS

This study of neotectonic (Pliocene – recent) structures comprises five complementary approaches: (1) Lineament analysis and (2) drainage analysis to define the regional fracture pattern, followed by (3) analysis of the volcano morphology, and (4) interpretation of remote sensing data (satellite images, air photos) and digital elevation model (DEM) imagery combined with (5) field work to verify the interpretations to infer the kinematics of the interpreted fractures.

5.1 Lineament analysis

5.1.1 Methodology

One common application of lineaments interpreted from satellite images is to reveal dominant azimuth sets whose orientations give an idea of the regional fracture pattern of an area (McElfresh et al., 2002, Casas et al., 2000, Koike et al., 1998). A lineament is defined geomorphologically as a "mappable, simple or composite linear surface feature, whose parts are aligned in a rectilinear or slightly curvilinear relationship and which differs distinctly from the patterns of adjacent features and presumably reflects a subsurface phenomenon" (O´Leary et al., 1976). Linear surface features may include valleys, ridges, boundaries of elevated areas, rivers, coast lines, boundary lines of rock formations, and fracture zones (Hobbs, 1904). The identification of lineaments is conditioned by the outcrop situation of the study area: The presence of dense vegetation, alluvial deposits, recent volcanic ashes and human landscape transformation may prevent the identification of lineaments.

5.1.2 Results and interpretation

Lineaments have been analyzed from the Landsat TM mosaic of the study area (Fig. 5.1). Lineaments are most significant within the Main Cordillera. In the Longitudinal Valley, human landscape transformation (agriculture, streets, and cities) prevents a geological meaningful lineament analysis from Landsat imagery.

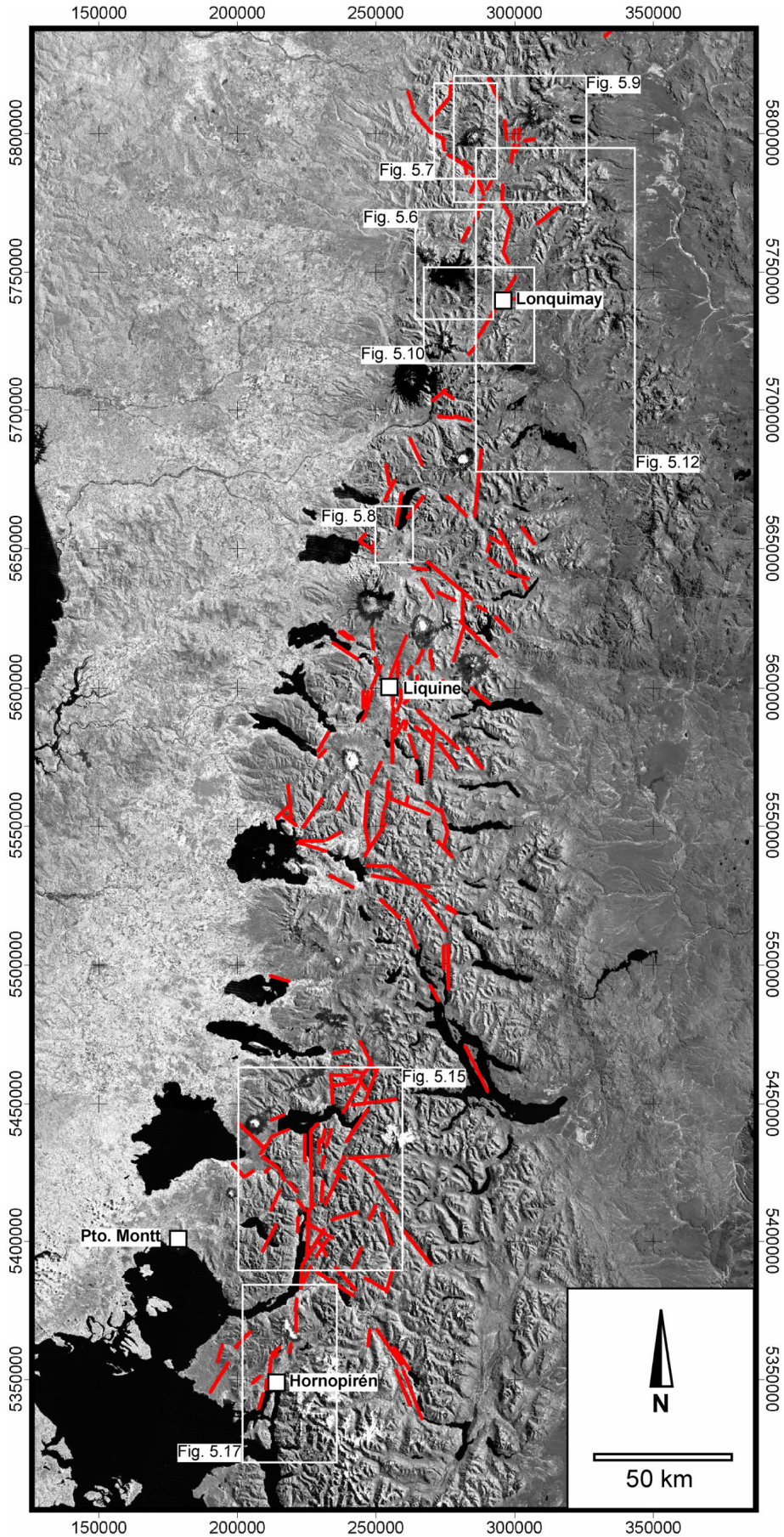

Fig. 5.1: *Lineaments of the Southern Andean intra-arc zone interpreted from Landsat TM imagery (UTM 19 S projection, PSAD 1956 ellipsoid).*

221 structural related lineaments have been recognized within the Main Cordillera between 37° and 43°S. Lineaments range in length from 1.8 to 27.5 km with a mean length of 7.6 +- 4.6 km (1σ standard deviation). Fig. 5.2 shows the distribution of lineaments in the study area. The main directions are: N10°E, N40°E, and N40°W. A minor direction is E-W. This lineament pattern is interpreted to reflect the pattern of upper crustal joints and faults. A Pliocene to recent age of the lineaments is inferred from the observation that they cut dominantly basement rocks and volcano-sedimentary deposits as young as Miocene and occasionally volcanic rocks of the Pliocene to active volcanic arc. In the next chapter, drainage network analysis has been used to give additional geomorphologic support to the definition of lineament sets derived from satellite image analysis.

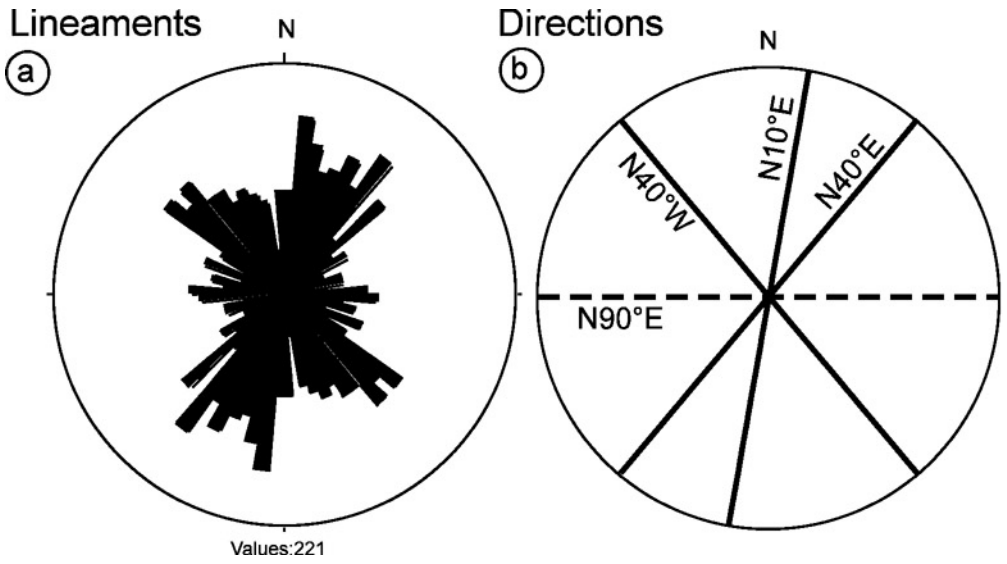

Fig. 5.2: *Results of lineament analysis from Landsat TM imagery: (a) Rose diagram and (b) dominant directions of lineament sets.*

5.2 Drainage analysis

5.2.1 Methodology

Drainage analysis generally provides clues to structural features and lithology (Howard, 1967). The underlying concept is that rivers necessarily flow from high to low elevations parallel to the maximum regional slope (regional topographic gradient). Several basic drainage patterns have been defined: dendritic, parallel, trellis,

rectangular, radial/centrifugal, annular, and contorted (Deffontaines and Chorowicz, 1991, Howard, 1967). All deviations from a dendritic pattern or flow direction oblique to the regional topographic gradient ("misfit drainage", Deffontaines et al., 1992), are considered as drainage anomalies related either to structural or lithological discontinuities (e.g. Deffontaines et al. , 1997, Pubellier et al., 1994). In this work, drainage analysis has been used to support the ideas of distinct lineament sets interpreted from satellite images.

Drainage analysis of an area generally starts with the individualization of areas of subhomogeneous drainage pattern ("subareas"). This individualization can be done on the basis of a regional analysis of the drainage pattern, stream flow direction, and drainage texture. Resulting subareas correspond more or less to the regional lithological units and bioclimatic zones (Deroin and Deffontaines, 1995, Howard, 1967). After individualization, detailed analysis of drainage anomalies brings out the perturbations that cannot be identified on a regional scale. Such regional perturbations consist of rectilinear or curved anomaly alignments.

The drainage pattern used in this work has been digitized from the 1:50.000-scale topographic maps of the IGM of Chile. It covers the segment of the Main Cordillera west of the watershed between 37° and 40°S comprising an area of about 26.000 km^2. The regional slope is to the west. Dry valleys resulting from erosion by streams which do not flow permanently have not been taken into account in this study. Lakes were considered by digitizing their shorelines.

5.2.2 Regional analysis

Subareas are differentiated in this work according to criteria of drainage pattern type, direction of stream flow, and drainage texture. Drainage texture can be expressed quantitatively on the basis of stream density which is the total length of watercourse per unit area (Deffontaines, 1990). A 5000 m-spaced grid of stream density has been derived from the digitized drainage using the following numeric routine: First, a grid overlay of the analyzed is designed and intersected with the vectorized drainage network to arrive at a set of drainage vectors which are segmented according the overlay grid. Second, the length of individual drainage vectors within each grid cell is calculated. Individual lengths are summed up for each cell and the obtained information is added to the overlay grid. Figure 5.3 a shows the result of this algorithm. Red colors correspond to relatively high stream densities/fine drainage texture, whereas blue colors correspond to low frequencies/coarse drainage texture.

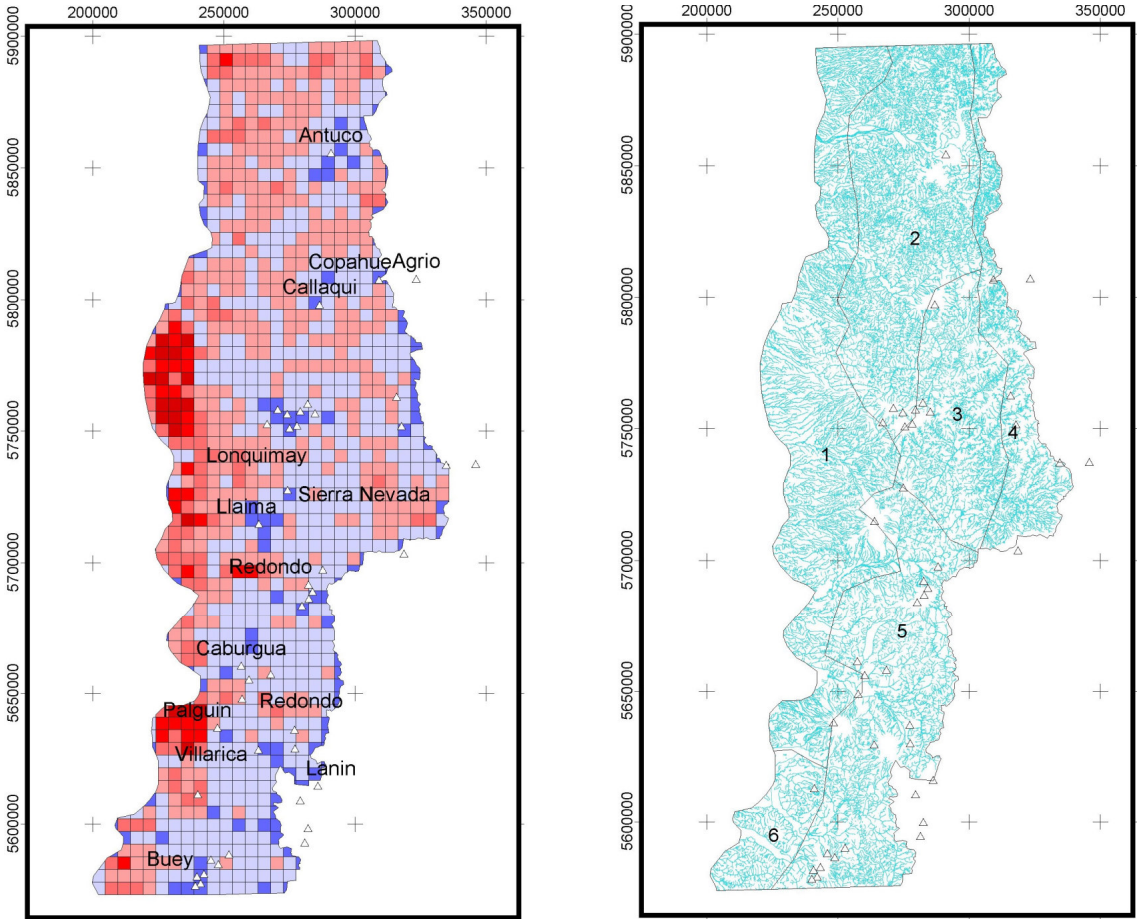

Fig. 5.3: *Results of regional drainage analysis: (a) Stream density of the Chilean Main Cordillera between 37° and 40°S as derived by numerical analysis of 1:25.000 drainage network (UTM 19 S projection, PSAD 1956 ellipsoid). Red = high density, blue = low density. (b) Subhomogeneous areas individualized based on stream texture, direction of stream flow, and drainage pattern type. Volcanoes are indicated by white triangles.*

5.2.3 Subarea individualization

Stream density calculation (Fig. 5.3 a) indicate variation in stream length per unit cell between 142 m and 251 km with a mean of 69 km. The most striking feature of the stream density map is exceptional high stream density along the western foothills of the cordillera. Generally, the northern part of the area is characterized by higher densities than the southern part. Small areas of low stream density comprise volcanic edifices (e.g. Vn. Antuco, Vn. Callaqui, Vn. Lonquimay, Vn. Llaima, Vn. Buey) and lakes (e.g. Laguna La Laja north of Vn. Antuco, Lago Caburga).

Subarea 1 comprises the western foothills of the cordillera north of Villarica with high stream densities/fine drainage texture. It displays dense parallel drainage pattern developed on relatively fresh and impermeable young volcanic material (e.g. Fm. Malleco). Flow direction is generally parallel to the regional slope, i.e. to the west with

a weak radial variation due to the shield like deposition pattern of volcanics around eruptive centers.

Subarea 2 is the northern part of the Main Cordillera and characterized by moderate to high stream densities/medium to fine drainage texture. The drainage pattern is dominated by the recurved trellis type with a tendency to dendritic pattern developed within folded and fractured volcano-sedimentary strata (Fm. Trapa-Trapa). Stream flow is directed mainly to the West subparallel to the regional topographic gradient.

Subarea 3 is the middle part of the Main Cordillera including the broad Biobío valley where weakly folded sedimentary rocks (Fm. Cura-Mallin) crop out. The drainage pattern is dominated by NW-SE striking tributaries to the NE-flowing subsequent Biobío river. This trellis type pattern is occasionally modified to recurved or directional trellis due to folds and halfgraben-like structures, respectively. Subarea 3 shows moderate stream densities/medium texture. Stream flow directions show a marked variance with a dominance of northerly directions normal to the regional topographic gradient.

Subarea 4 constitutes the near-watershed area in the north. There, where Pliocene basalts form a plateau (the Pino Hachado High), drainage pattern tends to be dendritic. Stream flow directions are to the West, subparallel to the regional slope. Stream density is moderate to high, corresponding to a medium to fine drainage texture.

Subarea 5 is the southern part of the Main Cordillera which is made up of dominantly granitoid basement of the North Patagonian Batholith (NPB). It shows moderate stream densities corresponding to a medium drainage texture. Drainage pattern here is of fault trellis type with a wider spacing than trellis in the northern subareas and with a tendency toward dendritic pattern between adjacent parallel subsequent streams. Stream flow direction is dominantly N-S normal to the regional slope or to the northwest.

Subarea 6 includes the southern foothills of the Main Cordillera comprising glacial lakes. Stream density is high according to a fine drainage texture. It shows contorted drainage patterns. Flow direction is towards the northwest.

Quaternary volcanism has modulated the regional drainage pattern described above in the whole study area in two ways: First, the volcanic edifice itself, which is circular to ellipsoidal, is dissected by radial to ellipsoidal drainage patterns. Second, volcanoes and lava flows forced existing drainage pattern to deviate from their old direction simply by representing a physical barrier. Emplacement of the Vn. Antuco in the north of subarea 1, for example, resulted in damming up the Laguna La Laja.

5.2.4 Drainage anomalies

Drainage anomalies considered in this work are straight sections of watercourses, oriented lakes, and aligned confluences. Fig. 5.4 shows the drainage network anomalies derived from analysis of the 1:50.000 hydrologic map.

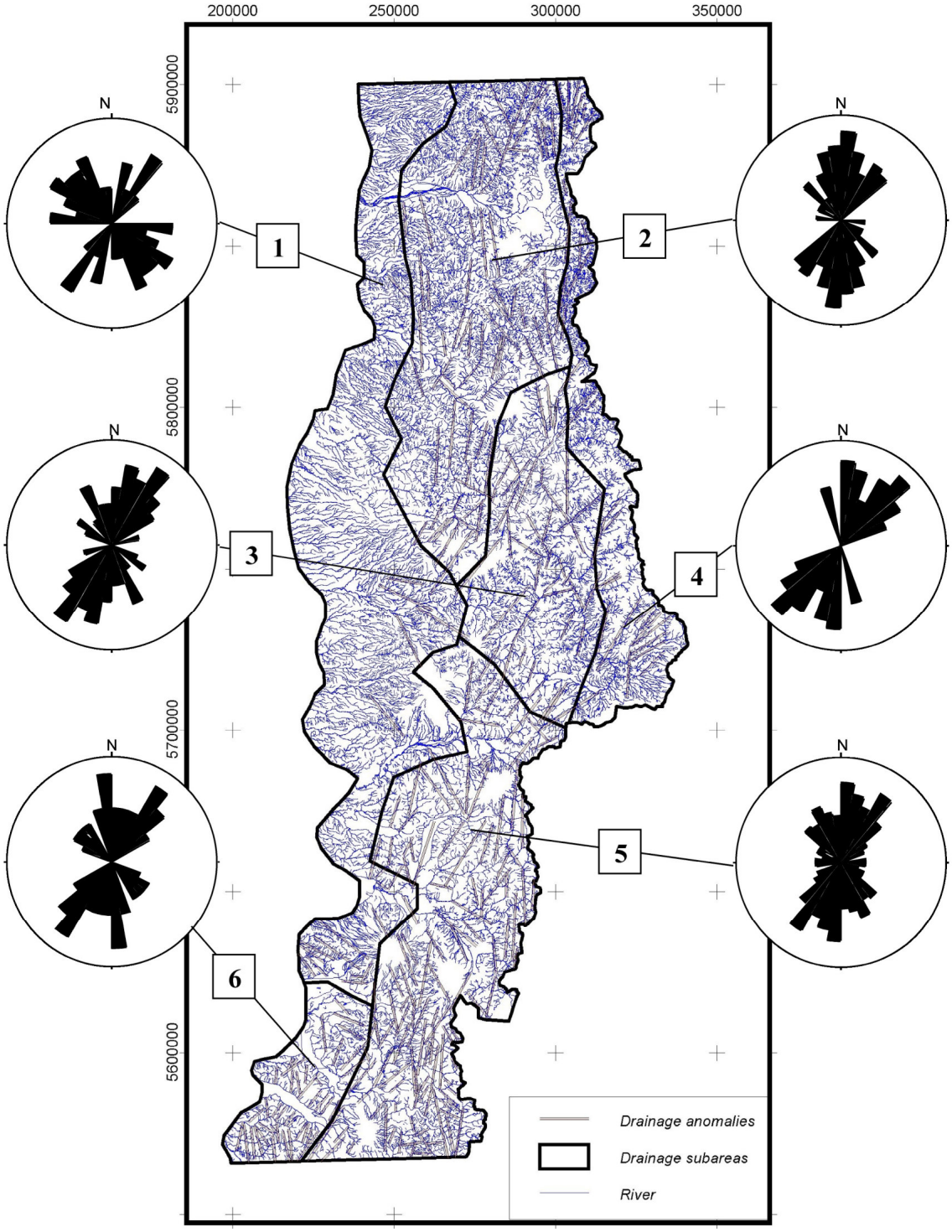

Fig. 5.4: *Drainage network anomalies (UTM 19 S projection, PSAD 1956 ellipsoid).*

Drainage anomalies occur in all subareas irrespective of the age of outcropping rock. The fact that the youngest rocks affected by drainage anomalies are of Pliocene age (Subarea 1 and 4) indicates their neotectonic significance. The major trend of drainage network anomalies in the study area is N-S to NE-SW in all subareas and all rock types. This argues that arc-parallel anomalies represent neotectonic features. Another trend observed in the study area is NW-SE.

Results of drainage network anomalies are consistent with results of lineament analysis (previous chapter). Both methods reveal the significance of N-S to NE-SW and NW-SE oriented lineament sets which are interpreted as subvertical fracture zones. E-W trending lineaments revealed from lineament analysis are not recognized using drainage network analysis because this direction is parallel to the regional topographic slope and consequently not considered as anomalous in the hydrologic sense. This pattern of arc-parallel and arc-oblique lineaments has been recognized by previous workers (e.g. Steffen 1944, Hervé, 1976, Munizaga et al., 1988, Muñoz, 1997). Their tectonic significance, however, remained incomplete: Whereas the arc-parallel lineaments are commonly related to the dextral Liquiñe-Ofqui Fault zone, the significance, age and kinematics of arc-oblique lineaments remained unknown. Most authors interpret them as inherited, probably pre-Andean discontinuities (e.g. Munizaga et al., 1988). In this work, a new interpretation is proposed, in that arc-oblique faults play a significant neotectonic role.

5.3 Volcanic fissures

5.3.1 Methodology

Nakamura (1977) introduced a method for obtaining the orientation of the principal tectonic stresses from volcanic surface features. The underlying concept is that volcanoes may be regarded as a large-scale natural magma-fracturing experiment. The method relies on the determination of dike swarms which are controlled by crustal-scale tension fractures (tension gashes). Those tension gashes open in the direction of minimum principal stress σ_3 (Fig. 5.5). The direction of subvertical dikes therefore corresponds to the maximum or intermediate principal stress accepting that the earths surface is a principal surface of stress (i.e., contains two principal stress axes) which may be valid in most upper crustal settings (Anderson, 1951, Engelder, 1993). In the absence of significant extension, the dike direction is the maximum principal stress σ_1.

The orientation of dikes feeding polygenetic volcanoes can be easily determined by mapping associated parasitic vents. In addition to the distribution of parasitic vents, elongation of the edifice of the volcano and the occurrence of normal faults within the volcanic edifice can be used to constrain dike orientation. Elongation of the volcanic edifice can result from the accumulation of volcanic material from parasitic vents. Normal faults may manifest dikes that did not reach the surface. For volcanic fields consisting of clusters of monogenetic cones, the alignment of monogenetic cones reflects the trend of dikes underneath.

Although, tectonic stresses may have the primary control on dike orientation (Delaney et al., 1986), it may also be influenced by gravitational stresses and/or the orientation of pre-existent basement fractures. To discriminate between tectonic stresses, gravitational stresses, and fault control on dike orientation, one has to carefully compare the orientation of parasitic cones with the basement topography and the spatial relationship with nearby faults.

5.3.2 Results and interpretation

Based on satellite images, air photos, geologic maps, and literature, I studied 56 volcanoes and volcanic fields of the Southern Volcanic Zone of the Andes (SVZ) between 37° and 42°S with respect to the distribution of monogenetic cones, elongation of the volcanic edifice, and their relation to faults. 42 of them show evidences for oriented dike swarms underneath (Fig. 5.5 and Tab. A2 in the Appendix II).

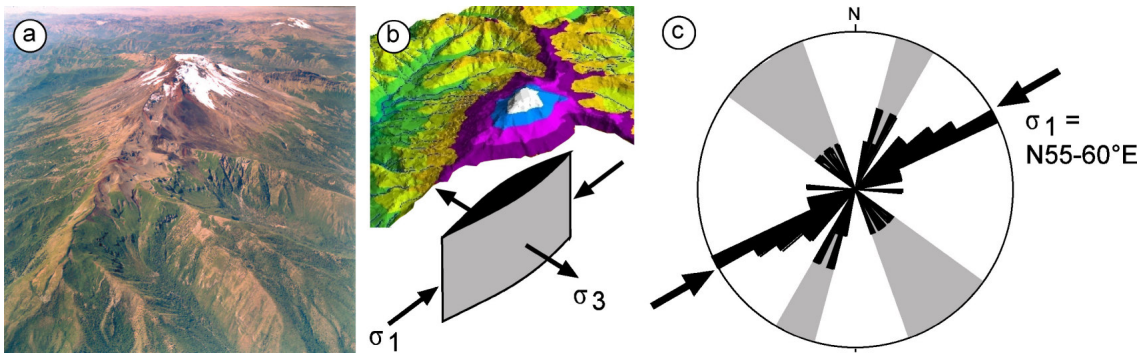

Fig. 5.5: *Concept and results of analysis of volcano morphology: (a) Oblique air photo of Vn. Callaqui (view to the NE); (b) conceptual model of an elongated volcano rooted on a tension fracture; (c) rose diagram showing the results of volcano morphological analysis (42 values, 5° interval).*

Most of the volcanoes show an elongation in NE-SW direction (N55°-60°E). Some of them are associated with arc-parallel faults. Other volcanoes show an elongation in NNE-SSW direction or NW-SE direction.

From the orientation of elongation and the relation of volcanoes to faults, four different mechanisms of extrusion are suggested: (1) volcanoes rooted on NE-SW oriented tail crack structures associated with arc-parallel strike-slip faults (e.g. Vn. Lonquimay, Fig. 5.6); (2) NE-SW oriented mega-tension gashes (e.g. Callaqui volcano, Fig. 5.5, 5.7), (3) NNE-SSW oriented tensional shear fractures associated with graben (e.g. Vn. Caburgua, Fig. 5.8) or pull-apart structures (e.g. Vn. Hornopirén, Fig. 5.17), and (4) NW-SE oriented tensional shear fractures related to reactivation of pre-existent basement structures (e.g. Vn. Tolhuaca in Fig. 5.6). In the absence of significant extension, type 1 and type 2 volcanoes are interpreted to be fed by dikes opening perpendicular to the maximum stress (σ_1). σ_1 in the Southern Andean intra-arc zone is thus inferred to have an orientation of N55-60°E. This is consistent with findings of previous authors (e.g., Nakamura, 1977, Sanhueza and Cembrano, 2000, López-Escobar et al., 1995). López-Escobar et al. (1995) showed that volcanoes related to NW-SE trending structures have chemically more evolved magmas (andesitic to rhyolitic) than volcanoes rooted on NE-SW trending structures (dominantly basaltic). They suggested that this is probably the result of longer crustal residence times of the more differentiated melts due to the compressional state of stress along NW-SE trending ascent paths (which are perpendicular to σ_1).

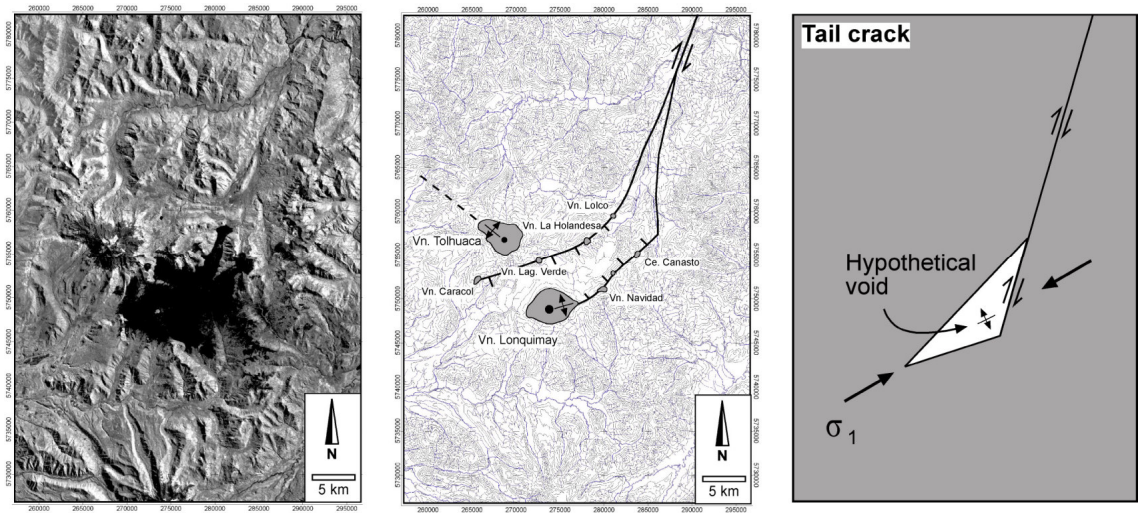

Fig. 5.6: *Vn. Lonquimay and Vn. Tolhuaca as examples of, respectively, NE-SW elongate volcanoes related to a tail crack structure of a dextral arc-parallel strike-slip fault and NW-SE elongate volcanoes rooted on pre-existent basement structures (UTM 19 S projection, PSAD 1956 ellipsoid).*

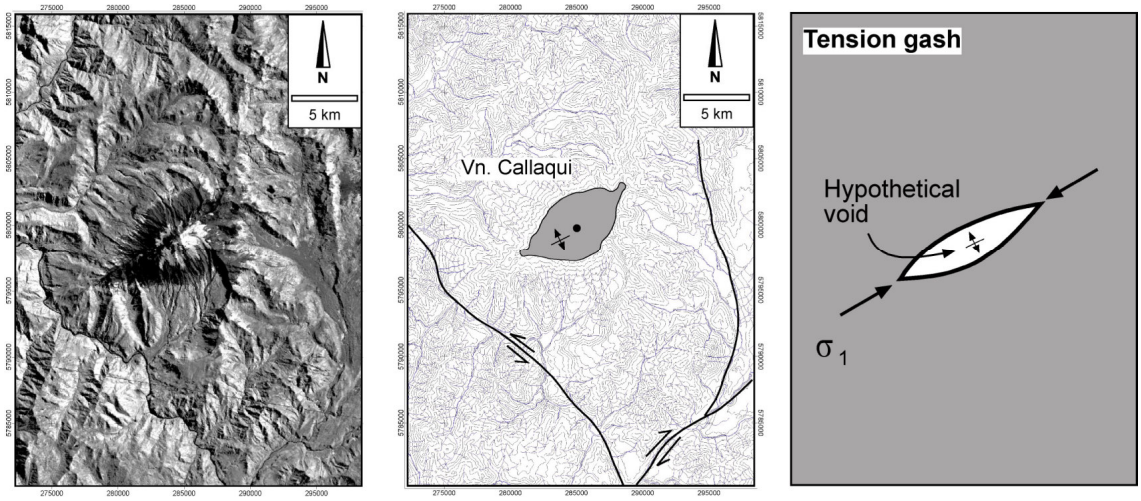

Fig. 5.7: *Vn. Callaqui as an example of a NE-SW elongated volcano rooted on a tension gash and not related to nearby faults (UTM 19 S projection, PSAD 1956 ellipsoid).*

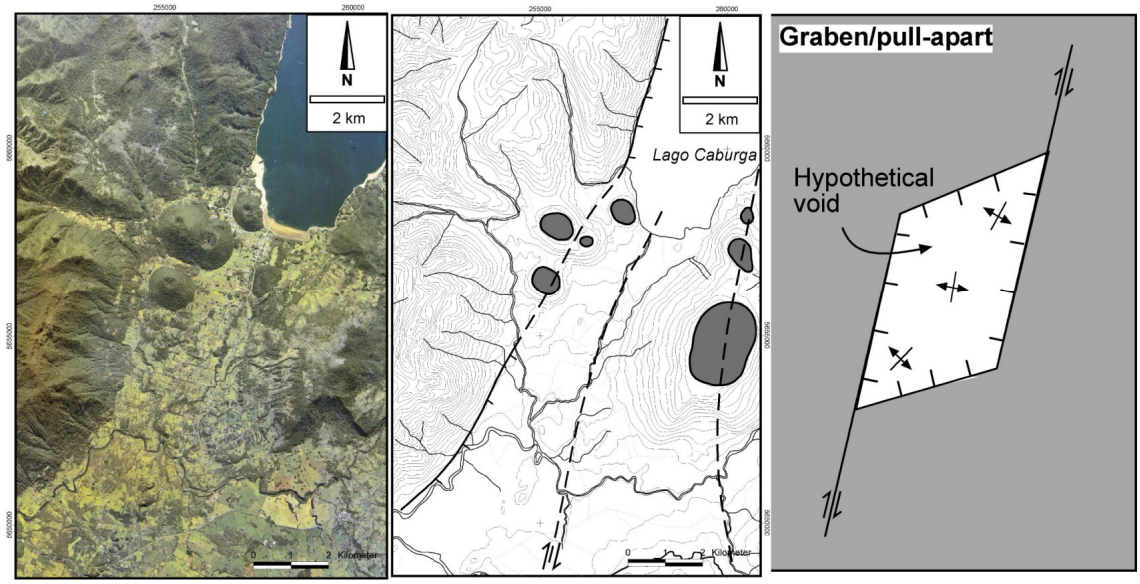

Fig. 5.8: *Volcanic field at Lago Caburga associated with a NNE-SSW oriented graben (UTM 19 S projection, PSAD 1956 ellipsoid).*

5.4 Fault scarps

5.4.1 Methodology

Fault scarps resulting from strike-slip faulting are generally well identified as distinct continuous straight lines several tens of kilometers in length and made up of a succession of aligned valleys. Strike-slip faults produce offsets of ridges and rivers and are often associated with typical patterns such as horse-tail and tail-crack structures. Normal fault scarps generally bound tilted blocks and are concave towards the

downgoing block and associated with a significant break in slope (landslides). Tilted blocks are expressed morphologically by asymmetric ridges separating opposite parallel type drainage systems. Scarps of thrust faults are generally subparallel to topographic isocontours and often associated with a moderate break in slope and anticlinal folding. Recent surface uplift related to faulting is indicated by triangular faceted ridge spurs. Satellite images and air photos have been systematically compared with geological maps in order to carefully separate fault scarps from scarps resulting from differential erosion of contrasting lithology. Elongate volcanoes and linear clusters of volcanic vents are generally associated with the direction of feeder dikes underneath (see Ch. 5.3.1). Those feeder dikes may be either interpreted as tension gashes parallel to the maximum horizontal stress or as reactivated basement faults.

5.4.2 Interpretations

Lago El Barco area

The Lago El Barco (Fig. 5.9) is located at the northern end of the LOFZ. Several sickle shaped blocks are observed in this area which are tilted around N-S striking axes due to movements along east and west dipping normal faults. Tilting is evident from asymmetric slope distribution across the blocks and asymmetric drainage pattern developed on them. The block-bounding normal faults join the northernmost branch of the arc-parallel Liquiñe-Ofqui fault (LOF) south the Lago El Barco. This horsetail-like termination is consistent with a dextral strike-slip character of the LOF (Melnick, 2000).

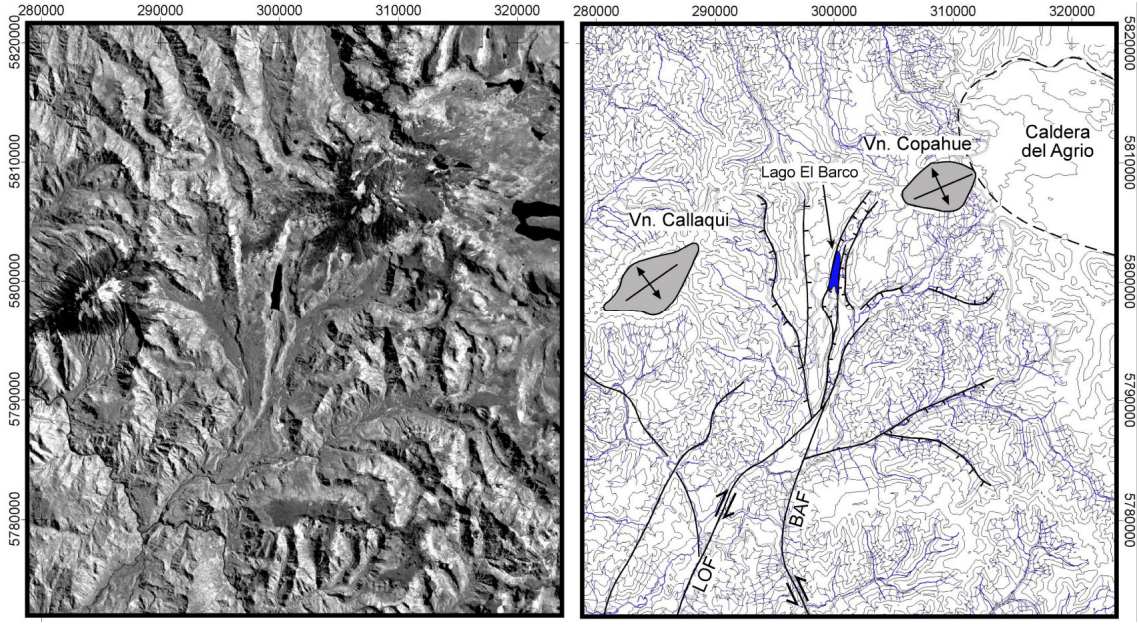

Fig. 5.9: *Satellite image and morphotectonic interpretation of the Lago El Barco area. Abbreviations: LOF = Liquiñe-Ofqui fault, BAF = Biobío-Aluminé fault. UTM 19 S projection, PSAD 1956 ellipsoid.*

Lonquimay area

The Lonquimay area includes two significant neotectonic features: (1) the Lonquimay valley and (2) the Cordillera Lonquimay. The Lonquimay valley is interpreted as a graben system composed of a NNE-SSW trending, ca. 20 km long and 3 km wide graben to the south of the town of Lonquimay and an E-W trending ca. 10 km long and 1-2 km wide graben to the east of Lonquimay (Fig. 5.10). Both grabens are filled with Quaternary fluvial deposits suggesting active subsidence. Mesoscale recent normal faulting is observed in this area (Fig. 5.11). The Lonquimay river meanders on the eastern side of the NNE-SSW trending graben. This suggests that the eastern part of the graben has subsided faster than the western part indicating a halfgraben structure with the main normal fault on its eastern side. The elongate Vn. Sierra Nevada is located in the southwestern prolongation of the southern end of the Lonquimay graben system indicating NW-SE oriented extension.

The mountain range south of Lonquimay, the Cordillera Lonquimay, consists of several tilted blocks bound by south dipping normal faults which join a southern branch of the LOF forming a horsetail structure. Tilting of the blocks is inferred from the asymmetry of drainage pattern following steep southern flanks and less steep northern flanks. This is supported by the observation of an E-W trending, 50-60° south dipping normal fault zone crosscutting Pliocene subvolcanic stocks in the north eastern part of the range. The occurrence of fault breccias with quarzitic matrix here indicates fluid circulation associated with fault activity. The geometry and kinematics of this horsetail structure is consistent with the dextral strike-slip character of the LOF.

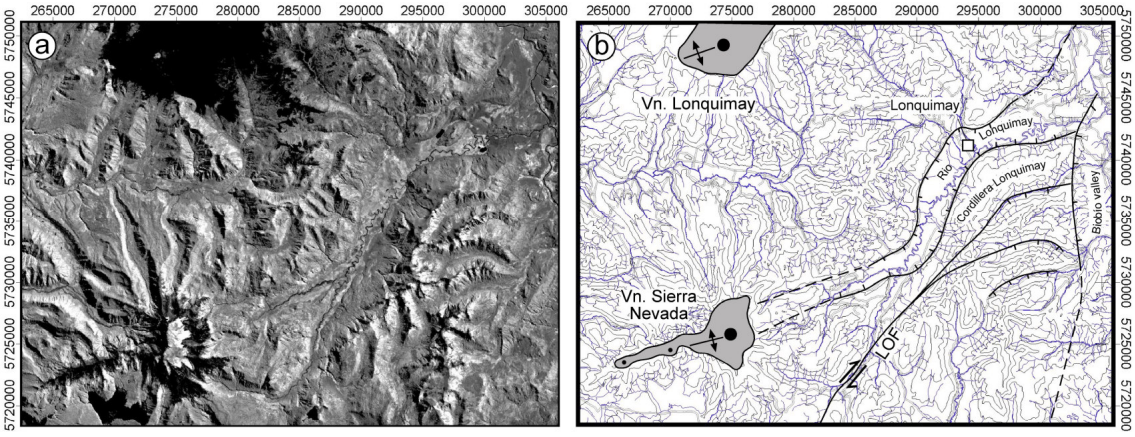

Fig. 5.10: *Satellite image and morphotectonic interpretation of the Lonquimay area. Abbreviations: LOF = Liquiñe-Ofqui fault. UTM 19 S projection, PSAD 1956 ellipsoid.*

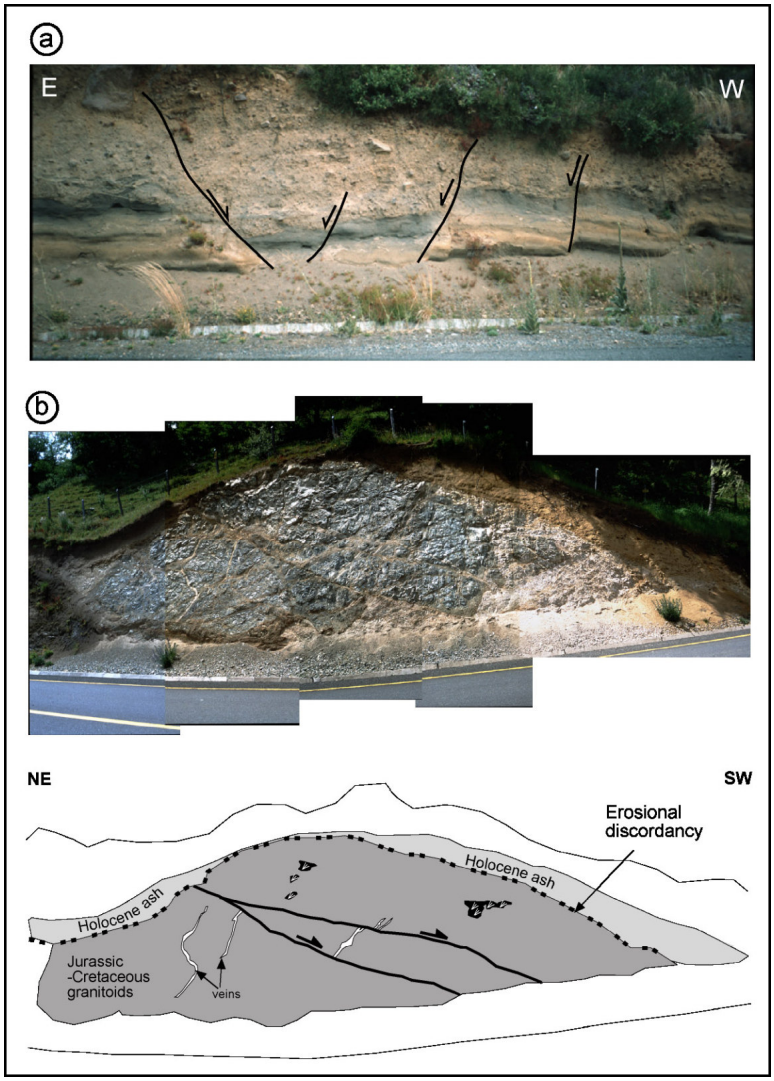

Fig. 5.11: *(a) Mesoscale graben affecting Holocene ashes (dark layer) and pre-Holocene normal faults (b) indicating E-W and N-S extension in the Lonquimay area.*

Biobío valley

The E-W trending graben of the Lonquimay graben system and the Lonquimay horsetail structure are cut by the Biobío valley in the east (Fig. 5.12). In the upstream area, the Biobío river meanders through a ca. 10 km wide NNW-SSE trending valley (perpendicular to the regional topographic trend) along a length of ca. 50 km. The valley floor is made up of Eocene to Miocene lacustrine sediments of the Fm. Cura-Mallín covered by few tens of meters of Quaternary fluvial deposits. Glacial deposits have not been observed in this valley (Suárez and Emparan, 1997). The western border of this valley is interpreted as a normal fault. The eastern border of the valley is represented by steep flanks with Pliocene plateau lavas on top. Some of the flanks are oversteepend as indicated by the occurrence of a large landslide in the center of the

valley (Suárez and Emparan, 1997). Mesoscale normal faulting has been observed within the Biobío valley indicating Pliocene to Pleistocene N-S extension (Fig. 5.13). This is consistent with the E-W elongation of the Trailihue volcano east of the Biobío valley. Stratigraphic work in the Cura-Mallín formation demonstrates the existence of faults with an east-up/west-down component in the eastern part of the valley (Kemnitz et al., in press), which could be interpreted as westward dipping normal faults. The BioBío-Aluminé fault (BAF, Suárez and Emparan, 1997) which runs through the Biobío valley has a slight bend in the area where normal faults occur. Therefore, the Biobío valley is interpreted as a fault-bend basin related to sinistral strike-slip movements along the BAF.

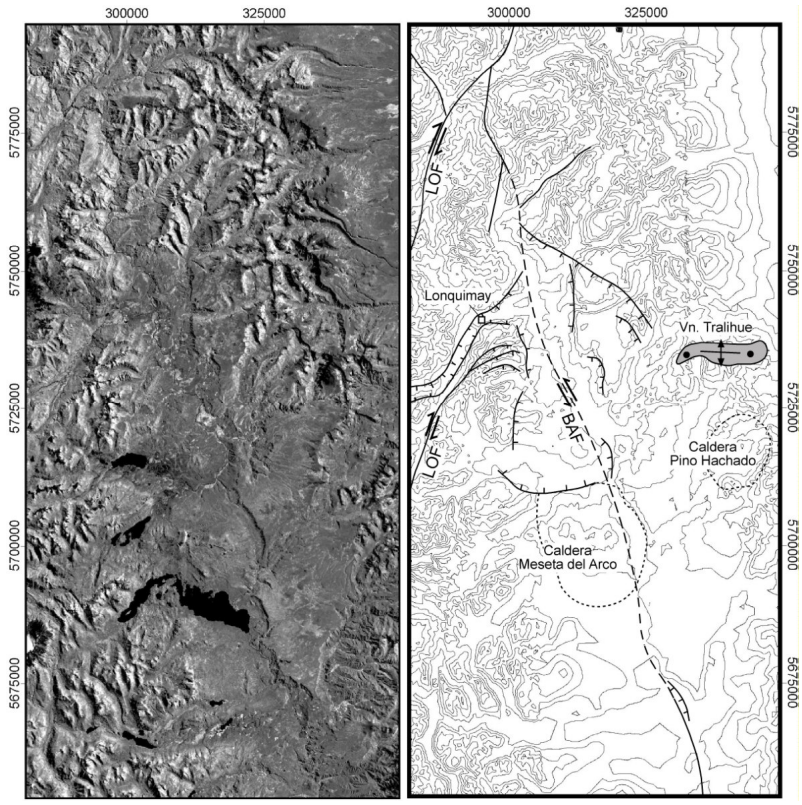

Fig. 5.12: *Satellite image and morphotectonic interpretation of the Biobío valley. Abbreviations: LOF = Liquiñe-Ofqui fault, BAF = Biobío-Aluminé fault. UTM 19 S projection, PSAD 1956 ellipsoid.*

In the northern part, the BBF runs through a narrow NNW-SSW to NW-SE trending valley and cuts into Jurassic to Miocene dominantly volcanic successions. Mesoscale flower-structures are observed along the valley flanks (Fig. 5.14) which crosscut Miocene sequences tilted during the Late Miocene inversion and thus indicate post-Miocene activity of the BBF. Silicate nodules observed close to the BBF trace suggest fluid circulation probably associated with fault activity. Microlayering observed in the nodules is still horizontal today indicating that no tilting is associated with movements along the fault. This is consistent with the proposed strike-slip character of the BBF.

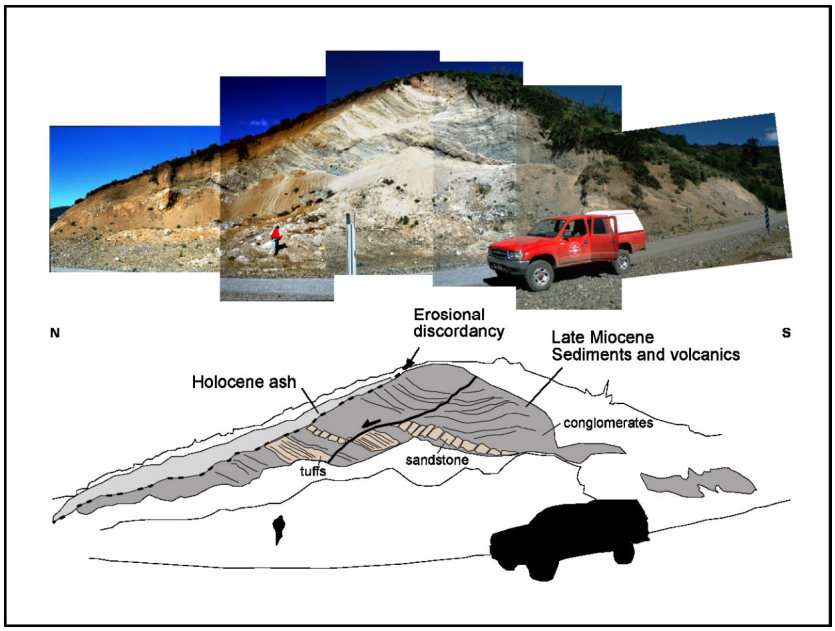

Fig. 5.13: *Mesoscale Pliocene-Pleistocene normal fault indicating N-S extension in the upper Biobío valley.*

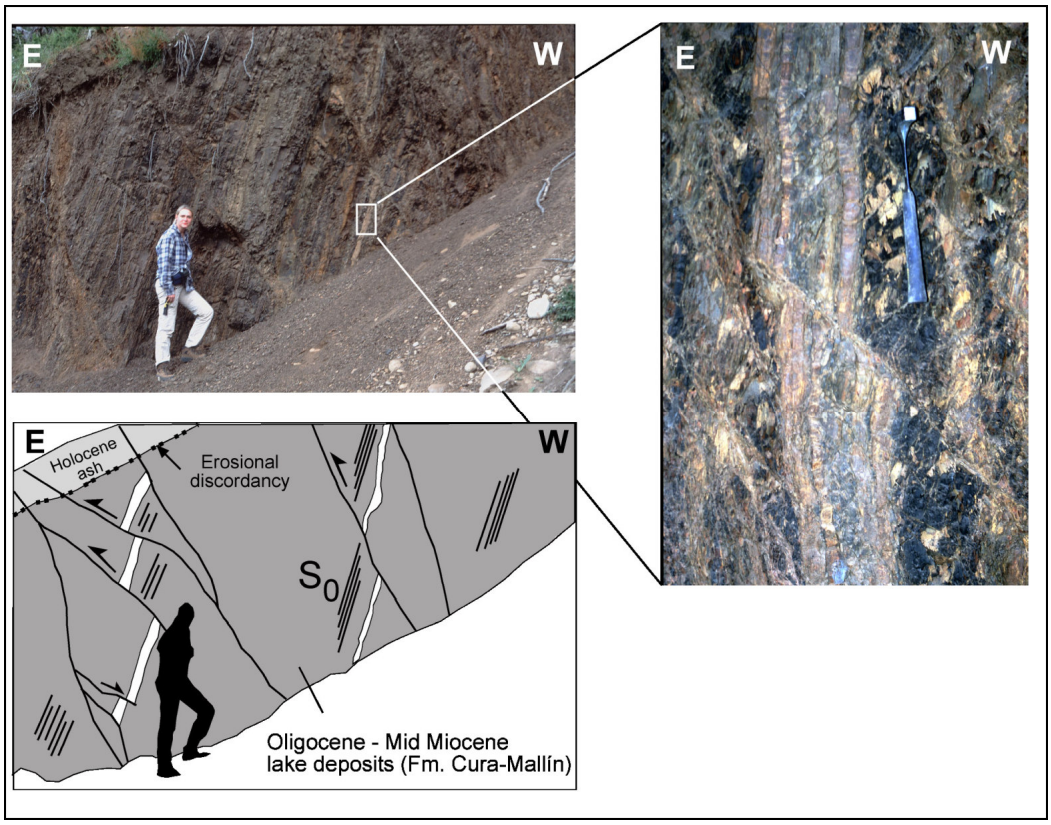

Fig. 5.14: *Post-Miocene faults with apparent inverse kinematics interpreted as part of a mesoscale flower structure in the Biobío valley.*

Lago Todos Los Santos area

Fig. 5.15 shows the morphostructural interpretation of the Lago Todos Los Santos area. The LOF is dextrally displaced across the Lago Todos Los Santos which itself is interpreted as a NE-SW to E-W trending graben. The Vn. Osorno is located on the normal fault bounding this graben to the north. It is rooted on a NE-SW oriented feeder dike system indicating NW-SE extension consistent with graben kinematics. The southern graben shoulder show facetted spurs indicating recent uplift (Fig. 5.16). In the central part, the LOF connects a southern elongate bay of the Lago Todos Los Santos with the Fj. Reloncaví. The Fj. Reloncaví itself is interpreted as a pull-apart basin bound by normal faults of the LOF. Monogenetic cones within the northern part of the fjord indicate E-W extension. An eastward bending trace SE of Cochamó is interpreted as a releasing splay of the dextral LOF. At Cochamó, another fault NNE-SSW trending fault branches off the LOF. Westward facing facetted spurs along a westward bend and eastward facing facetted spurs along an eastward bend suggest local transtension associated with this fault consistent with a dextral strike-slip character. At the northern end of the Fj. Reloncaví, another trace splits off the LOF to the NW. This fault displaces the westernmost part of the Todos Los Santos graben sinistrally and is associated with a normal fault component as indicated by triangular facets along a basin ward concave segment. Vn. Calbuco and Vn. Puntiagudo are not associated to faults. The latter is rooted on a NE-SW trending tension gash as indicated by its elongation.

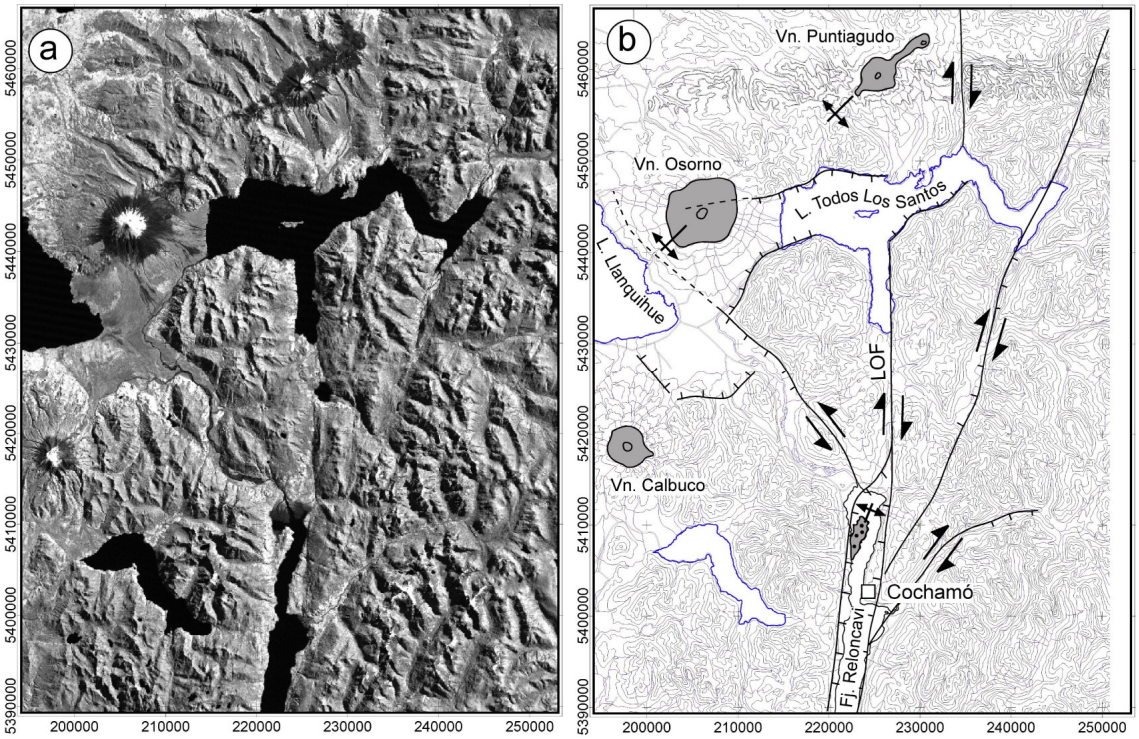

Fig. 5.15: *Satellite image and morphotectonic interpretation of the Lago Todos Los Santos area. Abbreviations: LOF = Liquiñe-Ofqui fault. UTM 19 S projection, PSAD 1956 ellipsoid.*

Fig. 5.16: *Facetted spurs south of Vn. Osorno indicating recent uplift of the mountain range.*

The Hornopirén area

Fig. 5.17 shows the morphostructural interpretation of the Hornopirén area. The dextral LOF is identified as a single trace north of the Vn. Hornopirén and splits into two branches south of it. Vn. Hornopirén shows a NNE-SSW elongation reflecting the orientation of feeder dikes. The two branches of the LOF are interpreted as normal faults bounding a pull-apart basin. Extension within the basin is oriented WNW-ESE as indicated by the feeder dike system of the Vn. Hornopirén.

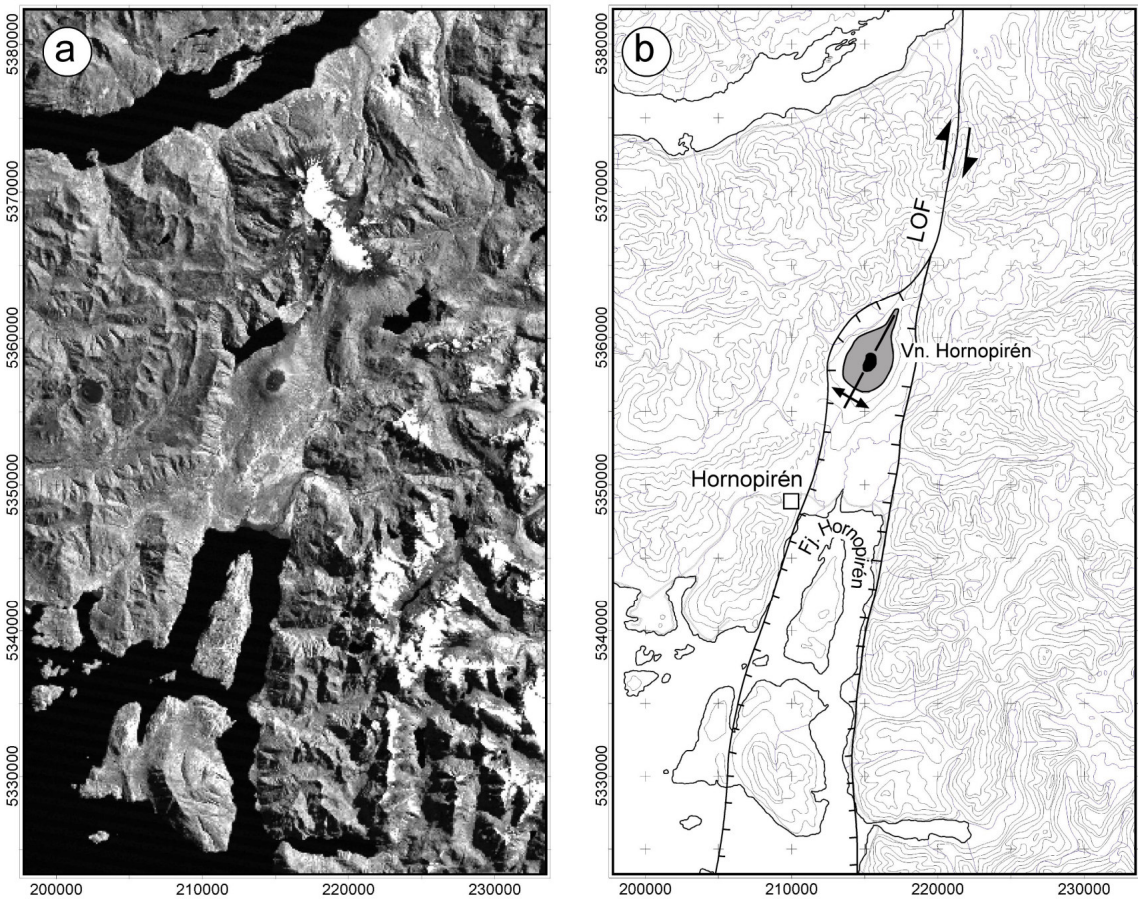

Fig. 5.17: *Satellite image and morphotectonic interpretation of the Hornopirén area. Abbreviations: LOF = Liquiñe-Ofqui fault. UTM 19 S projection, PSAD 1956 ellipsoid.*

5.5 Discussion

5.5.1 The LOFZ: a crustal scale SC-like fault zone system?

This neotectonic study shows that the LOFZ is more than a number of N-S striking dextral strike-slip faults. Moreover it is an 80 - 150 km wide fault zone system including dextral and sinistral strike-slip faults associated with horsetail structures, tailcracks, pull-apart basins, graben, and crustal scale tension gashes (Figs. 5.18 and 5.19). More specifically, the LOFZ is defined by two major systems of Pliocene to active faults which can be traced for tens of kilometers: Arc-parallel N to NE striking dextral strike-slip faults and arc-oblique W to NW trending sinistral strike-slip faults. The arc-parallel faults are generally associated with Pliocene to active volcanic centers in pull-apart basins and tailcracks. The curvature of individual strike-slip faults toward parallelism with antithetic strike-slip faults in some places and the mutual cross-cutting relationships between synthetic and antithetic faults in other places indicate that the two fault systems are geometrically and kinematically linked. More specifically, they define a crustal-scale shear zone with SC-kinematics (sensu Berthé et al., 1979, a conjugate set of two foliations which were synchronously formed during a single, progressive, non-coaxial deformation event). In that it is similar to the rhomb shaped tectonic segmentation of the Central Andean (Riller and Oncken, 2003) and Tibetian (Meyer et al., 1998) plateaus. Hippertt (1999) give further field examples of SC-like structures of crustal scale and demonstrated that SC-kinematics is a scale-invariant phenomenon (fractal) over ten orders of magnitude up to km-scale.

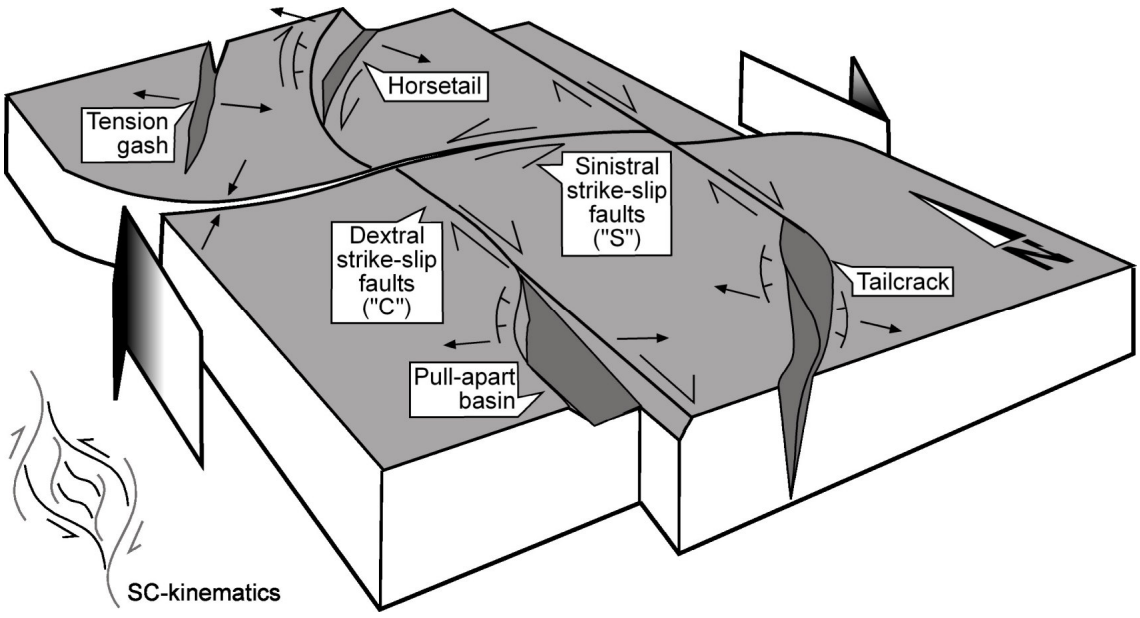

Fig. 5.18: *Conceptual model of the LOFZ with SC kinematics.*

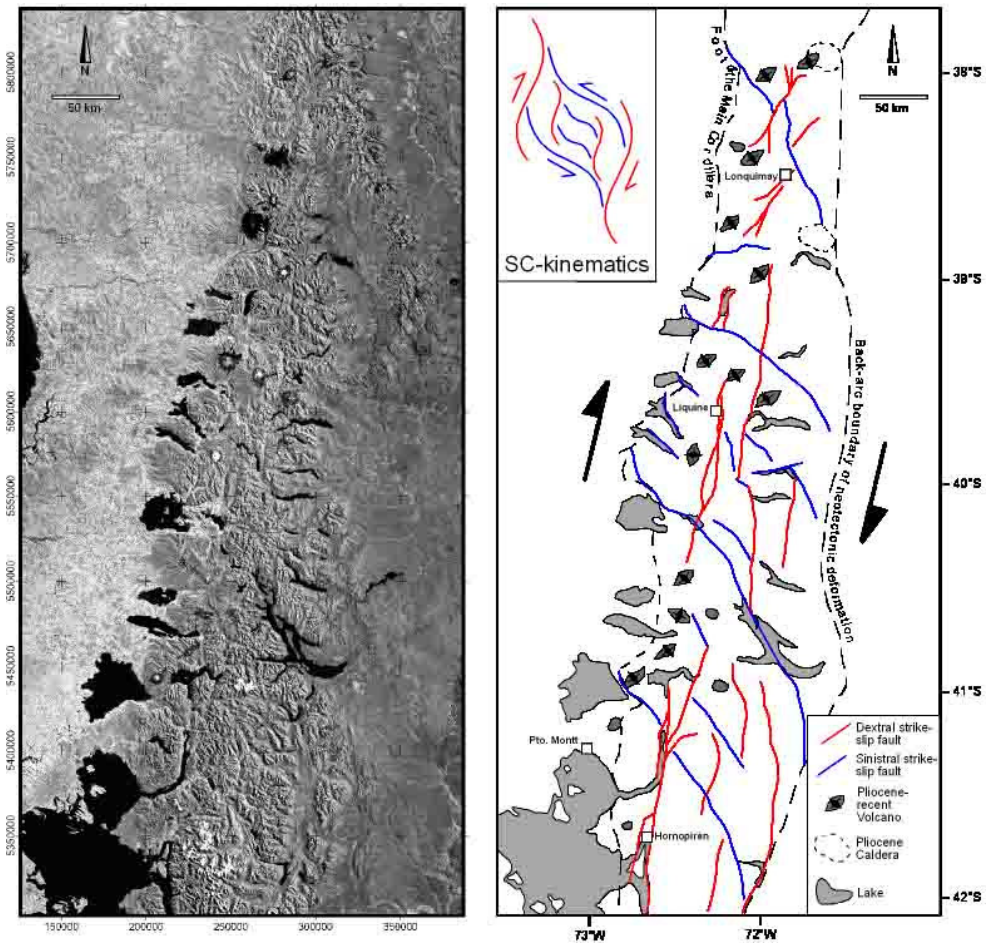

Fig. 5.19: *Neotectonic faults and fractures of the LOFZ between 38 - 42°S (Satellite image in UTM 19 S, PSAD 1956 ellipsoid).*

5.5.2 Reactivation of pre-existing discontinuities

As advocated for the Central Andean fault-and-thrust belt (Allmendinger and Gubbels, 1996) and plateau (Riller and Oncken, 2003), inherited structures have been important in localizing neotectonic deformation in the Southern Andes. The pre-Andean (Paleozoic - Early Triassic) structural grain of the area is characterized by NW-SE trending deformation zones parallel to the Gondwana margin defined by E-W to NW-SE striking foliation surfaces, thrusts, and strike-slip faults in the fore-arc (Martin et al., 1999) and by E-W to NW-SE trending foliation surfaces in the back-arc (Ch. 4.4.4, Rapela and Pankhurst, 1992). The Mesozoic to Tertiary structural grain is characterized N-S striking faults which controlled the geometry of basin bounding normal faults during Jurassic-Cretaceous and Eocene-Miocene phases of extension (Jordan et al., 2001, Pankhurst et al., 2000, Franzese et al., 2003, Dalziel, 1981) and the geometry of inverse faults and transpression zones during the Late Miocene (Ch. 4.6). As a consequence, pre-Andean and early Andean structures promoted the generation of, respectively, arc-oblique and arc-parallel fault zones in the Pliocene.

5.5.3 State of stress and stress partitioning

The upper crustal Pliocene to recent maximum stress σ_1 (which is parallel to the direction of instantaneous shortening) in the study area as inferred from the morphological analysis of volcanoes is oriented N55°-60°E. This is 45 ± 5° oblique to the volcanic arc which strikes N10-15°E. This geometry indicates the dominance of the simple shear component of crustal scale deformation consistent with the normal (i.e. neither thinned nor thickened) crust of the Southern Andes.

State of stress in the volcanic arc

To get constraints on the magnitude of stress within the intra-arc zone, a discussion based on the concept of Mohr circles (Mohr, 1900, 1904) and the Law of Effective Stress (*Terzaghi´s Law*, e.g. Secor 1965) follows. The latter states that the pressure of fluids in a rock reduces the normal stress on a fault plane in that rock. These concepts has been developed initially for brittle rock-fluid systems and has been successfully adapted to volcanic diking (Jolly and Sanderson, 1997) and even to magmatic underplating (Handy and Streit, 1999) demonstrating the universality of this approach.

Fig. 5.20 shows a family of two-dimensional Mohr circles, each one representing the surface plane stress conditions in the vicinity of one of three types of fractures differing in their strike direction and their relation to faults. Most volcanoes of the study area show an elongation in NE-SW and are interpreted to root on crustal scale tension gashes. Since these volcanoes are used to determine the σ_1 direction, they are a priori fed by feeder dikes which open perpendicular to σ_1. Fig. 5.20 a shows the Mohr circle for tension gashes, i.e. for fractures opening normal to σ_1. Purely extensional fractures indicate that, at least transiently and locally, differential stress (i.e. the difference between maximum and minimum stress; which equals the diameter of the respective Mohr circle)

$$\Delta\sigma < 4T \qquad \text{(E 5.1)}$$

(Secor, 1965), where T is the tensile strength of (isotropic) rock. Assuming an average value of 10 MPa for the tensile strength of crustal rocks (e.g. Etheridge, 1983, Kohlstedt et al., 1995), the differential stress during formation of tension gashes has to be lower than 40 MPa.

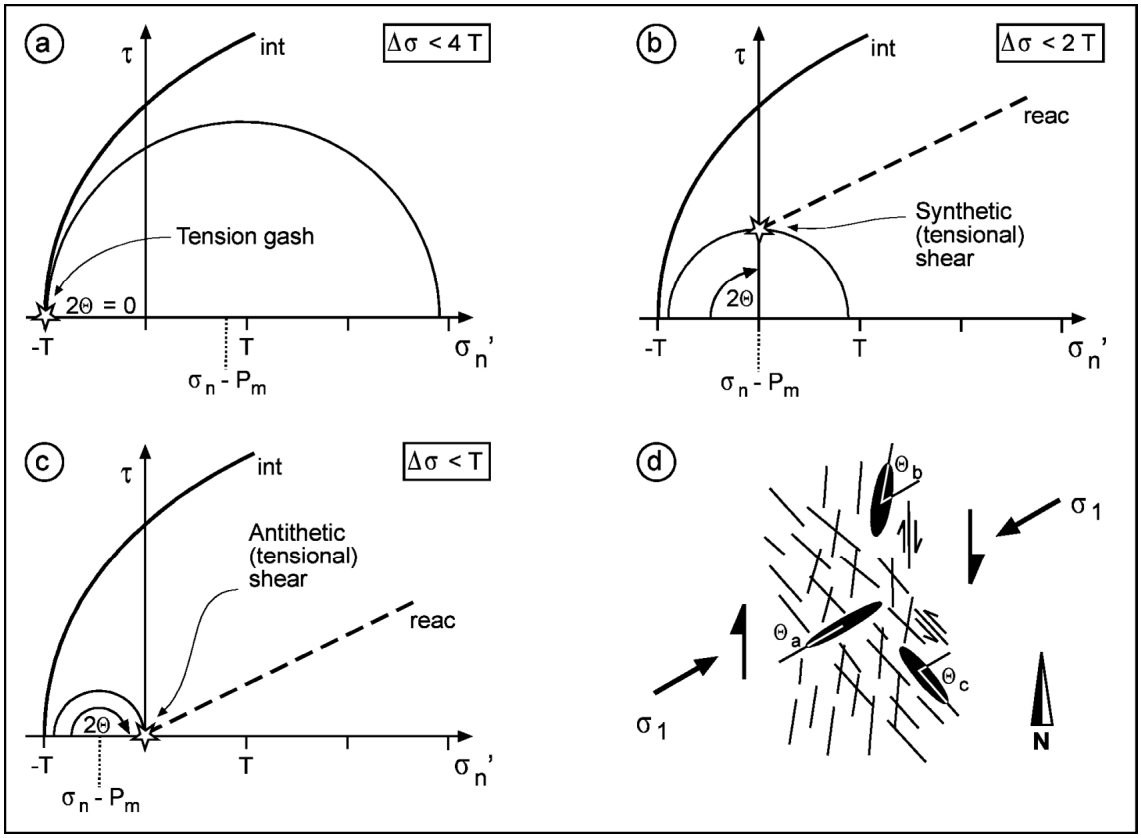

Fig. 5.20: *Mohr circle constructions for volcanic feeder dikes: (a) Tension gash, (b) tensional shear along arc-parallel faults, (c) tensional shear along arc-oblique faults, (d) geometrical relationships between stress and dikes. Griffith and Navier-Coulomb failure envelopes in the Mohr diagrams represent the strength of intact rock (int) and reactivated fractures (reac). Further abbreviations: τ - Shear stress on the fracture, σ_n – (effective) normal stress on the fracture, σ_1 - Maximum stress, $\Delta\sigma$ – differential stress, P_m – melt pressure, T – tensile strength of the rock, Θ - angle between dike and σ_1. See text for explanation.*

Not all volcanoes of the study area, however, are fed via dikes parallel to σ_1. There are also some volcanic feeder dikes oriented at angles between 45° - 90° to σ_1 (Fig. 5.5 c). The orientation of feeder dikes at such high angles to σ_1 is an unfavorable fracture orientation in isotropic rocks and requires the reactivation of pre-existing fractures for magma ascent (Sibson, 1985, Delaney et al., 1986, Jolly and Sanderson, 1997). For magma to open a pre-existing fracture, the melt pressure P_m must exceed the normal stress σ_n acting on the fracture walls:

$$P_m > \sigma_n \qquad \text{(E 5.2)}$$

Opening a pre-existing fracture at high angles to σ_1, i.e. $45° < \Theta < 90°$, is principally constraint by two factors: (1) the difference in strength between the intact rock and reactivated fracture, reflected by the distance between the respective failure envelopes in the Mohr diagrams ("int" versus "reac" in Fig. 5.20), and (2) the angle Θ between the dike and σ_1.

Figs. 5.20 b and c show the Mohr circles for volcanic feeder dikes reactivating pre-existent fractures parallel and oblique to the volcanic arc. Reactivation of arc-parallel fractures trending ca. 45 – 50° oblique to σ_1 (i.e. NNE-SSW trending dextral strike-slip faults) constrains the differential stress in the vicinity of these dikes to be

$$\Delta\sigma < 2T \qquad \text{(E 5.3)}$$

or, using the value of 10 MPa for T, less than 20 MPa (Fig. 5.20 b). Diking along pre-existing, arc-oblique fractures (i.e. NW-SE trending faults), which trend 80 – 90° oblique to σ_1 requires even smaller differential stresses limited by the relation:

$$\Delta\sigma < T \qquad \text{(E 5.4)}$$

i.e. differential stresses lower than ca. 10 MPa. To summarize, differential stresses in the Southern Andean upper intra-arc crust are variable and range between < 10 MPa and 40 MPa. This value is a reasonable constraint consistent with findings of other workers. Richardson and Coblentz (1994) and Coblentz and Richardson (1996) estimated, based on geodynamic modeling, a mean value of 20 – 25 MPa for the magnitudes of South American intraplate regional horizontal stress with local variations between 10 and 75 MPa. Force-balance calculations (Lamb and Davis, 2003, Yáñez and Cembrano, , 2004) suggest that the long-term strength of coupling between the Naszca and South American Plates, i.e. the shear stress transferred to the overriding plate, has have to be around 10 - 40 MPa in the study area during the Late Cenozoic to account for the observed lithosphere deformation.

Stress partitioning

The orientation of the maximum compressive stress in the intra-arc zone (N55-60°E) deviates significantly from the direction of Nazca-South American plate convergence vector which has been oriented ca. N75°E during the past 5 Ma (Somoza, 1998) as well as from the direction of absolute South American motion in a hot spot reference frame which changed from northwesterly direction to WSW 3 to 10 Ma ago (Marrett and Strecker, 2000). This marked deviation of stress directions across the Southern Andean margin contrasts with stress trajectories in the Central Andes which are subparallel to the Nazca-South American plate convergence and absolute South American plate velocity vectors (Assumpcao, 1992, Coblentz and Richardson, 1995). This indicates a high degree of partitioning of compressive stresses imposed by oblique convergence. A first-order factor controlling stress partitioning along the Andes is the thermally weakend intra-arc crust which may serve as a kind of “vertical detachment”, i.e. a

surface accommodating all applied stresses and thus representing a physical barrier across which no forces can be transferred into the back-arc.

However, the here inferred stress direction within the intra-arc zone may be valid only for the upper crust. Based on the statistic analysis of seismic moment tensor solutions, Apperson (1991) showed that intermediate-depth earthquakes (50 - 200 km) beneath the volcanic arcs of the world are mostly consistent with extension normal to the arc rather than with simple shear parallel to it. This may indicate that the deformation in the overriding plate is not only partitioned in horizontal plane but also vertically.